GEOPHYSICAL RESEARCH LETTERS, VOL. 22, NO. 2, PAGES 105-108, JANUARY 15, 1995

The 1993 Klamath Falls, Oregon, earthquake sequence: Source mechanisms from regional data

Jochen Braunmiller, John Nábělek, and Beate Leitner
College of Oceanic and Atmospheric Sciences, Oregon State University, Corvallis

Anthony Qamar
Geophysics Program, University of Washington, Seattle

Abstract. We use regional broadband seismograms to obtain seismic moment-tensor solutions of the two September 20, 1993, M_w=6, Klamath Falls, Oregon earthquakes, their foreshock and largest aftershocks (M_D>3.5). Several sub-groups with internally consistent solutions indicate activity on several fault segments and faults. From the estimated moment-tensors and depths of the main shocks and from the aftershock distribution we deduce that both main shocks occurred on an east-dipping normal fault, possibly related to the Lake of the Woods fault system. Rotation of T-axes between the two main shocks is consistent with the two dominant trends of the aftershocks and mapped faults. We propose that a change in fault strike acted as temporary barrier separating the rupture of the main shocks. Empirical Green's function analysis shows that the first main event had a longer rupture duration (half-duration 1.7 s) than the second (1.2 s). In December, vigorous shallow activity commenced near Klamath Lake's western shore, 5–10 km east of the primary aftershock zone. It appears a M_w=5.5 aftershock occurring the day before, though within the primary aftershock zone, triggered the activity.

Introduction

Two strong (M_w=6) earthquakes struck the Klamath Falls region of southern Oregon on September 20, 1993, at 8:28 pm and 10:45 pm local time (Figure 1). The epicenters (Table 1, Figure 2) were located 25 km northwest of Klamath Falls. Strong shaking produced ground cracking and landslides, but no surface faulting was found [*Wiley et al.*, 1993]. A foreshock (M_w=4.2) preceded the first main event by 12 minutes. The aftershock sequence is vigorous with more than 3000 events recorded during the following five months.

Klamath Falls is located at the northwestern-most edge of the Basin and Range province. The region is morphologically dominated by north- to northwest-trending normal-fault escarpments, some of Holocene age [*Hawkins et al.*, 1989]. Prior seismicity in the area has been, however, low. Only six earthquakes large enough to be felt occurred in the Klamath Falls vicinity during the 50 years preceding the 1993–94 sequence [*Sherrod*, 1993].

Installation of a sparse seismic network of three-component digital broadband stations in California, Oregon and Washington (Figure 1) has made possible source mechanism retrieval of moderate earthquakes (M≥4) using regional (Δ≤1000 km) waveforms [*Nábělek and Xia*, 1994]. This paper presents moment-tensor analyses of these data for 21 of the Klamath Falls earthquakes. We also show aftershock distribution located by the Washington Regional Seismic Network's (WRSN) local and regional stations; describe empirical Green's function estimates of source durations for the two main shocks; and conclude with a description of the space-time evolution of the entire sequence.

Copyright 1995 by the American Geophysical Union.

Paper number 94GL02844
0094-8534/95/94GL-02844$03.00

Aftershock Distribution

Because the nearest seismic stations were approximately 70 km from the earthquakes' epicenters, initial locations were biased 5–10 km to the northwest [*Qamar and Meagher*, 1993]. Deployment of portable stations by the U. S. Geological Survey and Oregon State University (OSU) and installation of permanent stations (Figure 2) in the epicentral region considerably improved later locations and allowed "master event" relocations of earlier events. Quality locations for events with M≥0.5 are available from Oct., 1993, on. More precise locations for the sequence's early stages will be possible when data from all portable stations are analyzed.

Figure 2a shows the aftershock activity between Oct. 6 and Dec. 3, 1993 (primary aftershock zone). Most activity occurs in the 4–12 km depth range. Aftershocks south of the first main shock (event 2) align in a northwest-trending pattern while aftershocks to the north show a north-south trend. Activity outside these two segments is limited. Cross-sections through various parts of the aftershock distribution do not reveal a fault plane. The dispersed seismicity may be a real phenomenon, but it is partially the result of inadequate depth estimate precision.

Installation of an additional station (HOG) in Jan., 1994, improved location quality. Figure 2b shows the aftershock activity between Dec. 4, 1993, and Mar. 10, 1994. Aftershocks continue

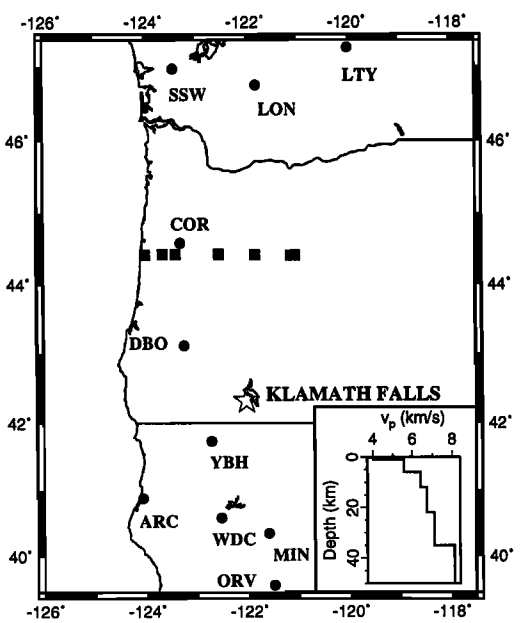

Figure 1. Map of epicentral area (star) and broadband seismic stations (circles and squares) used in this study. Squares: OSU temporary array in Oregon. DBO (Univ. of Oregon) was installed in the spring of 1994. Not shown are stations MHC, CMB, BKS, and STAN located further south. Inset shows the P-wave velocity/depth model used in this study.

Table 1. Epicentral and Source Parameters for Earthquakes Investigated in this Study.

Ev. #	OT date	h:m	Lat. (°N)	Lon. (°W)	S/D/R (°)	CD (km)	M_0 (Nm)		M_w	DC (%)	C #
1	930921	03:16	42.32	122.02	331/45/246	6	2.6	15	4.2	76	36
2	930921	03:28	42.32	122.03	331/47/255	9	1.1	18	6.0	96	39
3	930921	04:16	42.27	122.01	339/23/263	6	7.1	15	4.5	84	16
4	930921	04:34	42.30	122.03	320/50/243	6	3.6	15	4.3	88	18
5	930921	05:45	42.36	122.06	351/42/269	9	1.1	18	6.0	89	39
6	930921	06:14	42.39	122.05	355/52/259	5	2.1	16	4.9	83	21
7	930921	07:28	42.40	122.09	23/36/285	6	1.6	15	4.1	64	15
8	930923	06:21	42.30	122.04	353/46/266	6	7.4	15	4.5	46	36
9	930924	01:57	42.34	122.06	10/55/283	6	5.8	14	3.8	85	29
10	930924	16:53	42.37	121.94	330/38/256	3	1.2	15	4.0	93	28
11	930924	17:25	42.29	122.00	4/39/272	6	4.1	14	3.7	89	12
12	931130	03:30	42.28	121.99	304/56/247	6	2.5	14	3.6	84	12
13	931204	22:15	42.29	122.01	331/48/264	6–9	2.0	17	5.5	82	36
14	931204	23:50	42.23	121.96	7/26/25	6	1.2	15	4.0	97	15
15	931225	12:33	42.28	121.95	9/43/301	6	1.3	15	4.1	85	30
16	931231	18:08	42.29	121.94	8/25/290	3	1.8	15	4.1	79	24
17	940107	09:39	42.27	121.92	46/70/338	6	1.8	15	4.1	53	24
18	940108	02:55	42.25	121.92	55/62/338	3–9	6.1	14	3.8	97	30
19	940109	19:03	42.26	121.92	42/70/339	6–9	2.6	15	4.2	63	30
20	940119	22:27	42.29	121.95	346/34/269	6	1.7	15	4.1	55	24
21	940413	20:41	42.24	121.97	342/76/283	6	2.9	14	3.6	98	10

Ev.: event number. OT: origin-time. S/D/R: Strike, Dip, Rake. CD: centroid depth. M_0: seismic moment, integer number is exponent. DC: double-couple part of moment tensor. C: number of seismograms used for inversion.

to occur vigorously along the two segments active earlier with activity extending further southeast than before. Deeper events (blue) plot consistently east of shallower aftershocks (red) indicating an eastward fault dip for both main shocks. The most striking difference between Figures 2b and 2a is the vigorous, mainly shallow (0–8 km) activity near Klamath Lake's western shore, 5–10 km east of the primary aftershock zone. It appears the largest aftershock (event 13) occurring the day before the onset of this activity, though within the primary aftershock zone, triggered these events.

The aftershock distribution shown in Figures 2a and 2b, indicates activity on several fault segments and faults during the Klamath Falls sequence.

Regional-Waveform Inversion

We inverted seismograms recorded by regional broadband digital stations (Berkeley Digital Seismic Network, WRSN, and IRIS/OSU station COR; Figure 1) to obtain the seismic moment-tensor, source time history and centroid depth. For the smaller shocks we also used data from a temporary broadband array operated by OSU in western-central Oregon (Figure 1). The inversion procedure is described in *Nábělek and Xia* [1994].

We filtered complete three-component seismograms to a frequency band with good signal-to-noise ratio. For the main shocks and the largest aftershock we used frequencies between 0.01 to 0.05 Hz, for smaller events between 0.03 to 0.1 Hz. In these frequency bands the simple crustal model shown in Figure 1 provided an adequate match to the data. A 0.29 Poisson's ratio was chosen by matching waveforms at distant stations. All seismogram amplitudes were normalized to 100 km epicentral distance assuming cylindrical geometrical spreading.

Our analysis includes all events with M_D>3.5 except one event whose signal was contaminated by coda of event 13. Epicenters and source parameters for these 21 earthquakes are listed in Table 1. Fault plane solutions are shown in Figure 3. Within the source time function's resolution (~2 s), all investigated events had simple ruptures except event 11, which had two episodes of moment release separated by 10 s. The solutions do show definite variability, but they are consistent within different sub-groups, indicating activity on various faults.

As an example we show the match between observed (solid) and synthetic (dashed) seismograms for the second main shock (Figure 4). We observe large azimuthally-dependent amplitude variations tightly constraining the source mechanism. The ampli-

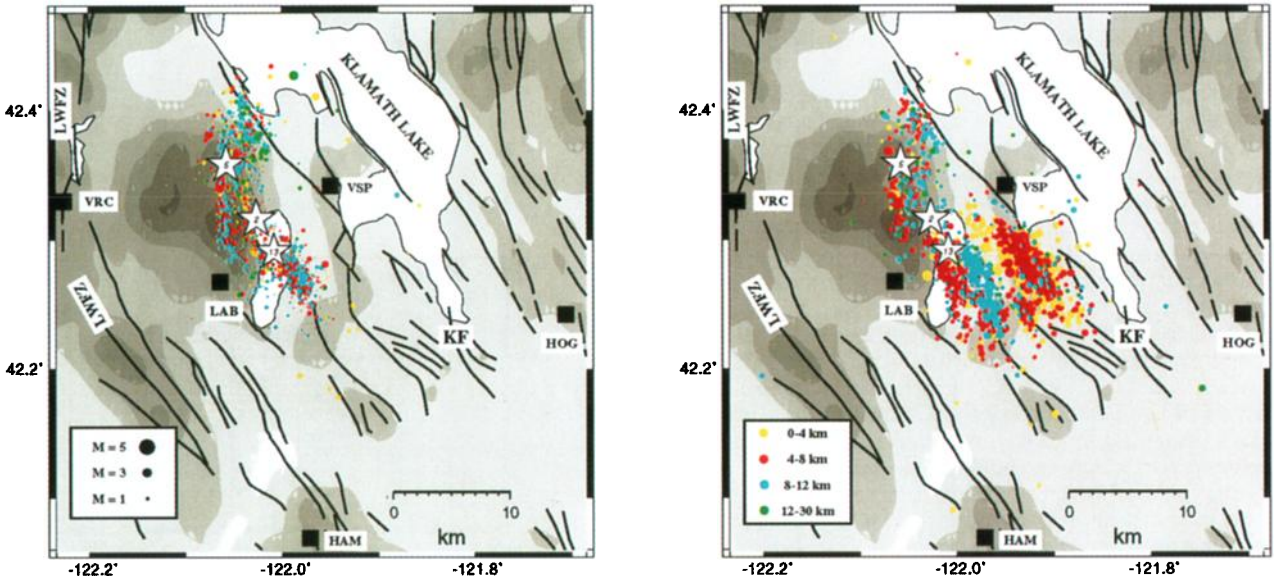

Figure 2. Aftershock locations. Deeper events plotted on top of shallower ones. Topographic contours in 200 m steps from 1000 to 2400 m (higher elevations darker). Fault traces are from *Walker and MacLeod* [1991]; LWFZ: Lake of the Woods fault zone. KF: Klamath Falls. Black squares are short-period stations of the Washington Regional Seismic Network installed in Oct., 1993; HOG installed in Jan., 1994. Stars mark locations of first (event 2) and second (5) main shock and of largest aftershock (13). a) Oct. 6 - Dec. 3, 1993. b) Dec. 4, 1993 - Mar. 10, 1994.

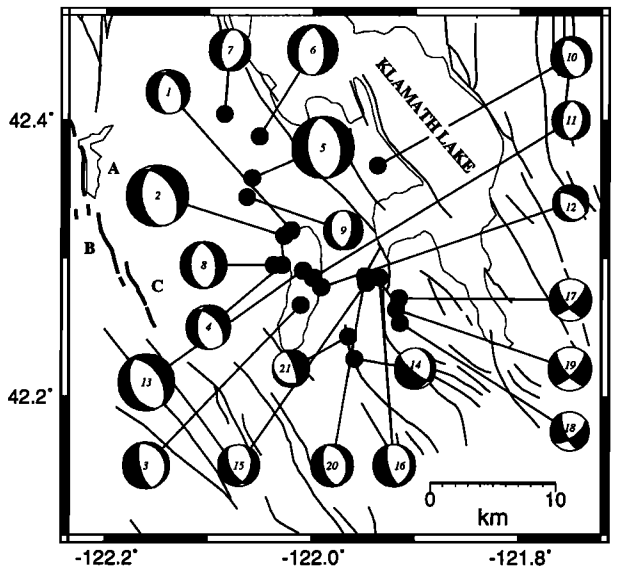

Figure 3. Locations of events studied (circles). Fault plane solutions (lower-hemisphere projections) with size proportional to M_w; numbers inside correspond to event numbers in Table 1. Bold fault traces of the LWFZ (marked A, B, C) are from high-resolution map of *Hawkins et al.* [1989].

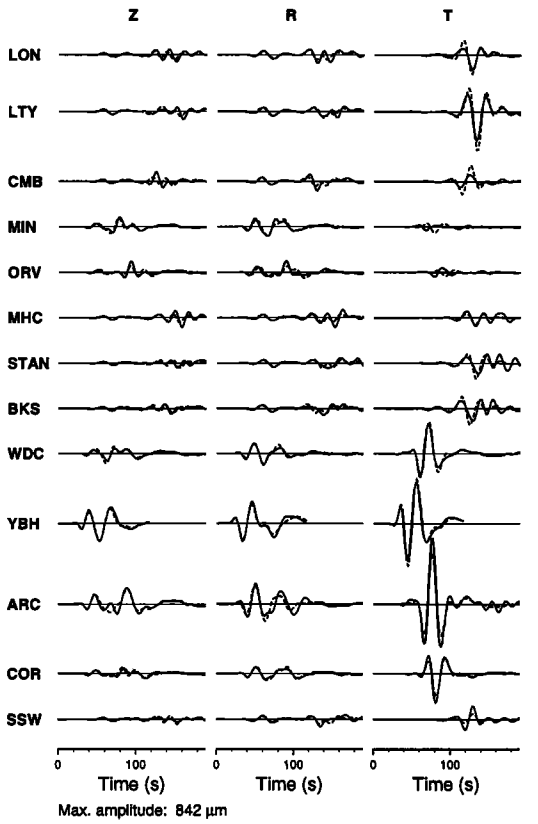

Figure 4. Observed (solid) and synthetic (dashed) seismograms for the second main shock (event 5). Z, R, and T are vertical, radial, and transverse components.

tudes of the observed seismograms are well matched and, except for nodal arrivals (transverse component at ORV and MIN), the waveform fit is also good.

The source parameters of the investigated earthquakes are generally well resolved. Figure 5a shows the variance as a function of centroid depth for the three largest events (2, 5, and 13). The centroid depths of the two main shocks are well resolved at 9 km, while the centroid depth of the largest aftershock is between 6 to 9 km. The fault plane solution of the second main shock is stable over a wide depth-range (Figure 5a). Figure 5b shows the resolution of the event's strike, dip and rake. Assuming an eastward dipping fault and a 9 km centroid depth, we find strike and rake are more tightly constrained than dip. Relative to the best-fit the bounds for a 5% increase in variance are ±1° for strike, ±2° for rake and ±5° for dip. For the aftershocks, bounds for a 5% variance increase average ±10° for strike, rake, and dip.

Empirical Green's Function Analysis

For the two main shocks we obtained source time function estimates by simultaneous deconvolution of three-component displacement seismograms. Aftershocks (events 1, 6, 8, and 9) located close to and with similar mechanisms as the main shocks were chosen as empirical Green's functions (EGF). The analysis was carried out individually for each station. In order to decrease the source duration estimates sensitivity to poorly resolved tails of low moment release, we describe results in terms of half-durations ($t_{1/2}$), the duration around the peak of the source time function during which 50% of the seismic moment was released.

Figure 6 shows these results. First main shock half-durations for stations towards south-southwest (WDC and YBH) are longer than towards north (COR) indicating northward rupture propagation. No consistent rupture directivity was found for the second main event; and the results depended strongly on the chosen EGF. The first event's average $t_{1/2}$ is 1.7 s, while the second main shock is shorter (average $t_{1/2}$ 1.2 s). Assuming a circular crack model [*Madariaga*, 1976] with equal rupture and healing velocities of 2.0 km/s, we obtain a rough estimate of rupture radius, average stress drop and average displacement of 3.4 km, 125 bar, and 85 cm for the first, and 2.4 km, 360 bar, and 105 cm for the second main shock. The aftershock distribution's extent for earlier aftershocks (Figure 2a) is consistent with these rupture dimensions.

Discussion and Conclusion

The Klamath Falls earthquake sequence is marked by a complex rupture history with several faults and fault segments being activated during different stages. Fault plane solutions (Figure 3) are dominated by normal faulting consistent with the region's extensional tectonics [*Hawkins et al.*, 1989; *Sherrod*, 1993]. The aftershock pattern (Figure 2) shows three general areas of activity: the northwest-trending southwestern zone where the foreshock, the first main event and the largest aftershock are located; the northern zone trending northward where the second main

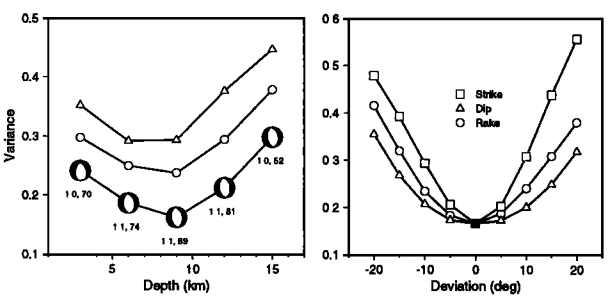

Figure 5. a) Variance vs. centroid depth. For event 5 estimates of the fault plane solution, seismic moment (in 10^{18} Nm, first number) and double-couple component of moment tensor (in %, second number) are shown for each depth. Circles: event 2; triangles: 13. For plotting purposes we added 0.05 to variances of events 2 and 13. b) Variance vs. deviation from best-fitting double-couple mechanism for event 5 for 9 km centroid depth.

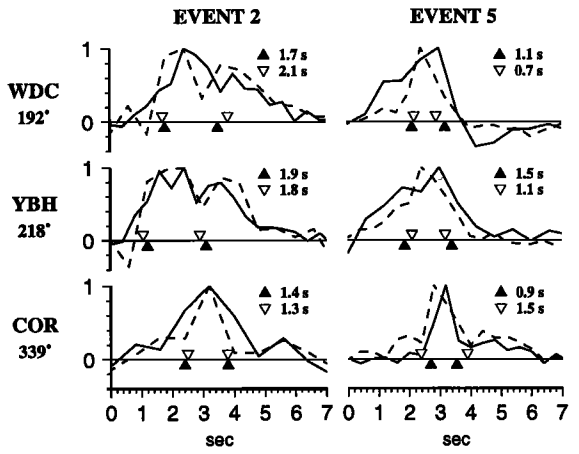

Figure 6. Far-field source time functions (normalized) from simultaneous deconvolution of three-component EGFs. First main shock (2): solid line, event 1 as EGF; dashed line, event 8 as EGF. Second main shock (5): solid line, event 6 as EGF; dashed line, event 9 as EGF. Half-duration estimates: filled triangles correspond to solid lines, open inverted triangles to dashed lines. Number beneath station code is station azimuth.

shock is located; and the eastern zone near Klamath Lake, activated on Dec. 4, 1993, trending northwest and dominated by shallow activity. The distribution of later aftershocks suggests that the two main shocks occurred on east-dipping fault planes.

The sequence started with a foreshock (event 1) followed 12 min. later by the first main shock (2). The epicenters of both events are adjacent. Larger aftershocks (3, 4) are displaced to the south-southeast. The second main shock (5) occurred two hours after and north of the first. In the following three days, aftershocks (6–9, 11) occurred in the primary aftershock zone. Event 10 is unusual; it falls in a region not very active throughout the entire earthquake sequence. Event 12 and the largest aftershock (13) occurred southeast of the first main event within the southwestern zone of activity. Events 14 and 21 are located at the southern tip of this zone. All other events (15–20) are located in the eastern aftershock zone. Here two distinct sub-groups are observed: the normal faulting earthquakes (15-16, 20) on the northern tip and the strike-slip events (17-19) on the southeastern edge.

The rotation of T-axes between the two main events and between events in the northern (5–7, 9) and southwestern (1–4, 8, 11–13) fault zones is well resolved as waveforms at several stations look distinctly different. The aftershock distribution and the mapped faults show a change from north-northwest trending to north trending in the vicinity of the first main shock's epicenter consistent with the T-axes rotation. Our waveform modelling results are consistent with those obtained by *Dreger et al.* [1994].

A direct association of the earthquakes to mapped faults is difficult at this time. For the two main shocks the causative fault possibly was the eastward-dipping Lake of the Woods fault zone (LWFZ, Figures 2 and 3) [*Hawkins et al.*, 1989]. The LWFZ reaches the surface approximately 10–12 km west of the main shock epicenters and undergoes a change in trend consistent with the moment tensor results. Surface projections of 45° eastward dipping fault planes passing through the main shocks' hypocenters (10 km, WRSN) are close to the LWFZ's surface trace. However, no shallow seismic activity has been recorded close to the trace. Shallow aftershocks are located several kilometers eastward, implying aftershock activity is confined to the hanging wall.

An interesting question is why the main rupture occurred as two M=6 earthquakes close in space and time instead of one M=6.2 earthquake. We propose that fault segmentation controlled the main rupture episodes. High-resolution map of *Hawkins et al.* [1989] shows that the LWFZ forms three distinct segments (A, B, C; Figure 3) in the epicentral region. The relative locations and mechanisms of the two main shocks and the largest aftershock are broadly consistent with the following scenario: the first main shock (event 2) initiated near the step-over separating segments C and B, propagated northwestward along segment B (Figure 3), and stopped near the fault bend separating segments B and A. The second main shock (event 5) occurred along the north-trending segment A. The largest aftershock (event 13) appears to have occurred on segment C. Initiation and termination of earthquake ruptures at geometrical barriers (e.g. fault bends and step-overs) has been observed for many earthquakes [e.g. *King and Nábělek*, 1985]. *Scholz* [1990] presents a model of "subcritical crack growth" to explain re-initiation of temporarily arrested ruptures across a barrier which could explain the delayed nucleation of the second main shock and possibly most of the aftershock sequence. However, the shift of activity to the eastern fault zone following the largest aftershock requires a different mechanism, probably involving stress relaxation within a complex fault zone as response to the main events. Interestingly, many recent continental normal faulting earthquakes occurred as sequences of two or more large shocks with comparable magnitude (e.g. Dixie Valley-Fairview Peak/Nevada, 1954; Corinth/Greece, 1981; Ethiopia, 1989), possibly reflecting intrinsic segmentation of normal fault systems as postulated by *Jackson and White* [1989].

Acknowledgements. Comments by J. Ritsema and two anonymous reviewers helped to clarify the text. This research was supported by the U.S. Geological Survey grant 1434-93-G-2326. Operation of broadband stations in Oregon was supported in part by grants from the Oregon Department of Geology and Mineral Industries and the National Science Foundation (EAR-9207181).

References

Dreger, D., J. Ritsema, and M. Pasyanos, Broadband analysis of the 21 September, 1993, Klamath Falls Earthquake Sequence, submitted to *Geophys. Res. Lett.*, 1994.

Hawkins, F.F., L.L. Foley, and R.C. LaForge, Seismotectonic study for Fish Lake and Fourmile Lake dams, Rogue River project, Oregon, *Seismotectonic Report 89-3*, 26 pp., U. S. Bureau of Reclamation, Denver, Col., 1989.

Jackson, J.A., and N.J. White, Normal faulting in the upper continental crust: observations from regions of extension, *J. Struct. Geol.., 11*, 15-36, 1989.

King, G.C.P., and J.L. Nábělek, The role of bends in faults in the initiation and termination of earthquake rupture, *Science, 228*, 984–987, 1985.

Madariaga, R., Dynamics of an expanding circular fault, *Bull. Seis. Soc. Am., 66*, 639–666, 1976.

Nábělek, J., and G. Xia, Moment-tensor analysis using regional data: application to the 25 March, 1993, Scotts Mills, Oregon, earthquake, *Geophys. Res. Lett.*, in press, 1994.

Qamar, A., and K.L. Meagher, Precisely locating the Klamath Falls, Oregon, earthquakes, *Earthquakes and Volcanoes, 24*, 129–139, 1993.

Scholz, C.H., *The Mechanics of Earthquakes and Faulting*, 439 pp., Cambridge University Press, 1990.

Sherrod, D.R., Historic and prehistoric earthquakes near Klamath Falls, Oregon, *Earthquakes and Volcanoes, 24*, 106–120, 1993.

Walker, G.W., and N.S. MacLeod, Geologic map of Oregon, scale 1 : 500 000, *U. S. Geological Survey*, 1991.

Wiley, T.J. , D.R. Sherrod, D.K. Keefer, A. Qamar, et al., Klamath Falls earthquakes, September 20, 1993 - including the strongest quake ever measured in Oregon, *Oregon Geology, 55*, 127–134, 1993.

Jochen Braunmiller, John Nábělek, and Beate Leitner, College of Oceanic and Atmospheric Sciences, Oregon State University, Ocean Admin Bldg 104, Corvallis, OR 97331-5503. (jbraunmi@oce.orst.edu)

Anthony Qamar, Geophysics Program, University of Washington, Seattle, WA 98195. (tony@geophys. washington.edu)

(Received July 20, 1994; accepted August 27, 1994.)